Chemosphere 360 (2024) 142457

Contents lists available at ScienceDirect

Chemosphere

journal homepage: www.elsevier.com/locate/chemosphere

Response surface methodology directed modeling of the biosorption of progesterone onto acid activated *Moringa oleifera* seed biomass: Parameters and mechanisms

Emily Ngeno [a,b,c], Roselyn Ongulu [a], Victor Shikuku [b], Deo Ssentongo [c], Benton Otieno [d], Patrick Ssebugere [c,e,f,*], Francis Orata [a,**]

[a] Department of Pure and Applied Chemistry, Masinde Muliro University of Science and Technology, P.O Box 190–50100, Kakamega, Kenya
[b] Department of Physical Sciences, Kaimosi Friends University, P.O Box 385–50309, Kaimosi, Kenya
[c] Department of Chemistry, Makerere University, P. O Box 7062, Kampala, Uganda
[d] Department of Chemical and Metallurgical Engineering, Vaal University of Technology, Vanderbijlpark, South Africa
[e] Department of Cell Toxicology, Helmholtz Centre for Environmental Research–UFZ, 04318, Leipzig, Germany
[f] Department of Analytical Environmental Chemistry, Helmholtz Centre for Environmental Research–UFZ, 04318, Leipzig, Germany

HIGHLIGHTS

- *MOSB* has been used in sequestration of progesterone (PGT) from solution.
- Optimum adsorbate parameters were 86.8 min, 500 μg L^{-1}, 298 K and 0.1 g dosage.
- PGT removal from aqueous solutions was pH independent.
- Biosorption of PGT onto *MOSB* was a spontaneous and exothermic process.
- Biosorption mechanism was physisorption and devoid of electrostatic interactions.

GRAPHICAL ABSTRACT

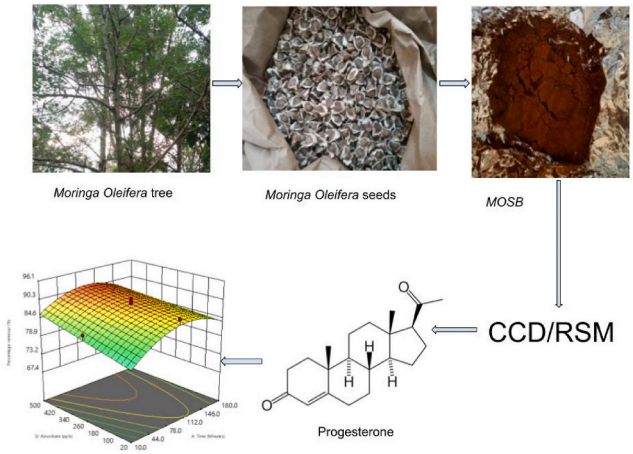

ARTICLE INFO

Handling editor, Charuvila T Aravindakumar

Keywords:
Moringa oleifera seed biomass (MOSB)
Progesterone

ABSTRACT

In this study, chemically activated fat-free powdered *Moringa oleifera* seed biomass (*MOSB*) was synthesized, characterized, and utilized as a cost-effective biosorbent for the abstraction of progesterone (PGT) hormone from synthetic wastewater. Natural PGT is a human steroid hormone from the progestogen family. Synthetic PGT is approved for the regulation of the menstrual cycle, aiding contraception, and is administered as a hormone replacement therapy in menopausal and post-menopausal women. PGT is an endocrine disrupting chemical

* Corresponding author. at: Department of Chemistry, Makerere University, P. O Box, 7062, Kampala, Uganda.
** Corresponding author.
E-mail addresses: patrick.ssebugere@mak.ac.ug (P. Ssebugere), fomoto@mmust.ac.ke (F. Orata).

https://doi.org/10.1016/j.chemosphere.2024.142457
Received 18 September 2023; Received in revised form 11 April 2024; Accepted 25 May 2024
Available online 27 May 2024

Acid-activation
Biosorption

(EDC) with negative health impacts on biota. The X-ray diffractogram (XRD), Scanning electron microscopy-Energy-dispersive X-ray spectroscopy (SEM-EDS), and Brunauer–Emmet–Teller (BET) analyses displayed a porous, amorphous biosorbent with an elemental composition of 72.5% carbon and 22.5% oxygen and a specific surface area of 210.0 $m^2\ g^{-1}$. The process variables including temperature (298–338 K), pH (2–10), contact time (10–180 min), adsorbate concentration (20–500 μg L^{-1}), and adsorbent dosage (0.1–2.0 g) were optimized using response surface methodology (RSM) to obtain the greatest efficacy of *MOSB* during biosorption of PGT. The optimum parameters for PGT biosorption onto *MOSB* were: 86.8 min, 500 μg L^{-1} adsorbate concentration, 298 K, and 0.1 g adsorbent dosage. PGT removal from aqueous solutions was pH-independent. The Langmuir isotherm best fitted the equilibrium data with maximal monolayer biosorption capacity of 135.8 μg g^{-1}. The biosorption rate followed the pseudo-first-order (PFO) kinetic law. The thermodynamic functions ($\Delta G < 0$, $\Delta H = -9.258$ kJ mol^{-1} and $\Delta S = +44.16$ J mol^{-1}) confirmed that the biosorption of PGT onto *MOSB* is a spontaneous and exothermic process with increased randomness at the adsorbent surface. The biosorption mechanism was physisorption and was devoid of electrostatic interactions. The findings from this study indicate that *MOSB* is an inexpensive, low-carbon, and environmentally friendly biosorbent that can effectively scavenge PGT from aqueous solutions.

1. Introduction

Progesterone (PGT) is a naturally occurring human steroid hormone from the progestogen family. Synthetic PGT is approved for the regulation of the menstrual cycle by correcting dysfunctional uterine bleeding or amenorrhea. It also aids with contraception by facilitating the implantation of the blastocyst in the uterus and sustaining the pregnancy. PGT has also been recommended and administered as part of hormone replacement therapy in menopausal and post-menopausal women (Almazrouei et al., 2023; Ojoghoro et al., 2021). It is introduced into the environment through human excretion, and mainly via effluent release from wastewater treatment plants (WWTPs), untreated biosolids from WWTPs applied as fertilizer in farmlands (Ngeno et al., 2023), and seepage from septic tanks and landfills (Golovko et al., 2018; Moulahcene et al., 2015). Multiple studies have detected progestogens in surface water (Almazrouei et al., 2023; Chang et al., 2011; Golovko et al., 2018; Šauer et al., 2018) including in effluents from various WWTPs in Kenya (Ngeno et al., 2023).

In the environment, PGT is known to be an endocrine disrupting chemical (EDC) with negative health impacts on biota. Synthetic progestogens have been reported to cause disorders in fish by affecting the sexual development of offspring, reducing egg production, and decreasing the spawning rate via increasing masculinity in female fish (Almazrouei et al., 2023; Golovko et al., 2018). Furthermore, zebrafish exposed to PGT showed altered liver function and ocular growth in addition to neurodevelopmental consequences (Almazrouei et al., 2023). Due to the ecotoxicological effects of PGT, its removal from water is monumentally significant. Physicochemical treatments such as flocculation, coagulation, and settling processes do not effectively abstract PGT (Kasonga et al., 2021; Ng et al., 2021; Orata, 2018), while advanced techniques like reverse osmosis, nanofiltration, oxidation processes, and membranes are expensive for developing countries due to high energy use, and intensive capital investment is required due to toxic waste material generated during the processes (Jayan et al., 2021; Mukherjee et al., 2021).

The quest for innovative cost-effective solutions for eliminating hazardous contaminants from wastewater has focused on biosorption. The biosorption technology is cheaper and flexible, with low energy requirements and a high rate of regeneration of the biosorbents. This simpler technique is based on the binding capacities of various biological materials and agro-industrial waste to pollutants (Ahalya et al., 2006). These carbonaceous porous adsorbents can be used as powdered materials, biochar, activated carbons, or carbon nanotubes. These biosorbents can be used with or without thermal and chemical modification (Ngeno et al., 2022).

During the biosorption process, the percentage removal is dependent on operational processes such as temperature, pH, contact time, initial concentration, and biosorbent dosage. The biosorbent characteristics playing a key role include its morphology, functional group type and density, hydrophobicity, and surface pH (Salame and Bandosz, 2003). These properties are dependent on the biomass type, and the activation conditions (Chimi et al., 2023). Biosorption efficiency is also affected by the adsorbate characteristics such as polarity, hydrophobicity, kinetic diameter, and dissociation pattern (Shikuku et al., 2018). A super biosorbent exhibits high biosorption capacity, fast kinetics, adsorbs a wide range of pollutants, and is inexpensive (Ngeno et al., 2022).

Traditionally, the biosorption process is investigated by varying one operating factor while holding other variables at an unspecified or specified constant level. The limitation of this is that it does not consider the synergistic or antagonistic effect, if any, of all the variables involved. Furthermore, it is costly both time-wise and in the use of reagents, and optimal conditions are not guaranteed (Jayan et al., 2021; Ong et al., 2011). These can be avoided by using statistical experimental designs such as response surface methodology (RSM). RSM is a multivariate approach for designing experiments, modeling, evaluating factor interactions, and collectively optimizing all parameters affecting biosorption (Ani et al., 2019; Korde et al., 2021) thus giving the system's ideal operating conditions or an area that meets the optimum operational specifications. The use of RSM in biosorption has been noted to be cost-effective while improving biosorption efficiency, reducing process variability, and determining the significance of each process parameter, if any, in controlling adsorbent performance (Aly-Eldeen et al., 2018; Ani et al., 2019).

The biosorbent in this study was *Moringa oleifera (M.O)* seed biomass. *M.O.* is a tropical tree that can withstand drought and is available all year round. It has medicinal applications such as analgesic, anti-inflammatory, and antihypertensive properties, as well as weight loss (Grosshagauer et al., 2021; Jayan et al., 2021). In terms of nutritive value, the *M.O* leaves and seeds are loaded with vitamin C, protein, potassium, and calcium (Anwar et al., 2007). Besides the foregoing uses, numerous research has explored the capability of different parts of *M.O* (bark, leaves, seed, and seed pods) as a biosorbent for the sequestration of contaminants from aqueous solutions and have reported positive results. Imran et al. (2019) reported 98.6% removal of Pb^{2+} ions while Jayan et al. (2021) reported 95.6 and 89.4% removal of Pb^{2+} and Zn^{2+} ions, respectively, both using unmodified leaves of *M.O*. Keereerak and Chinpa (2020) reported 86.2% removal of crystal violet dye using pod husks, while Maina et al. (2016) and Ongulu et al. (2015) reported high removal efficiencies of heavy metals (i.e., Pb, Cd, Cu, Mn, Fe, Zn, Mg and Cr) using acid treated seed pods.

Few studies have investigated PGT removal using biosorption. Ragab et al. (2016) reported 95.0% of PGT removal using polytetrafluoroethylene (PTFE) double-layer microfiltration membrane modified with zeolite imidazolate metal-organic frameworks-8. Moulahcene et al. (2015) reported 98.2% removal of PGT using cyclodextrin polymers cross-linked with citric acid. Another study by Ghasemi et al. (2017) demonstrated that 4 g L^{-1} of PGT required 10 g cellulose (no percent given), whereas Ifelebuegu et al. (2016) reported a 60.0% PGT removal

using UV photo-assisted Fenton-like degradation. The paucity of studies shows that the removal of PGT has not received considerable attention. To the best of our knowledge, the acid-activated, fat-free *M.O* seeds have not been investigated for the removal of PGT from aqueous solutions with RSM as an experimental design tool for the optimization of process parameters.

The goals of this study were to (i) determine the adsorptive capability of acid-activated *M.O* seeds in adsorbing PGT from aqueous solutions, (ii) optimize the process parameters using RSM, and (iii) evaluate biosorption dynamics through modeling. The biosorption kinetics, thermodynamics, and general mechanistic studies were also investigated and are herein reported.

2. Materials and methods

2.1. Standards, chemicals, and reagents

A reference standard for PGT was purchased from Sigma Aldrich. NaOH and HCl (analytical grade) were purchased from Kobian Kenya Limited. Ultrapure water was obtained from Milli-Q gradient ultrapure water system.

2.2. Pretreatment of the adsorbent

M.O seeds were purchased from Nakasero market, Kampala, Uganda. The seeds were manually de-shelled before pretreating as reported by Ongulu et al. (2015) but with modification as given in Text S1. The sample was labeled *MOSB*.

2.3. Characterization of MOSB

The surface chemistry of *MOSB* was determined by investigating its pH at a point of zero surface charge (pH_{pzc}). The pH_{zpc} measurements were obtained using the pH drift method (Text S2). To obtain the sample crystallinity of *MOSB*, a Bruker D8 Advance X-ray diffractometer (XRD) with copper Kα monochromator at the voltage of 15 kV, scanned at a wavelength (λ) of 1.54 Å with 2θ angle range from 5° to 90° was used. Morphology, microstructure, and percentage elemental composition of *MOSB* were obtained by scanning electron microscopy–energy dispersive spectroscopy (SEM-EDS) (JSM-IT500). Fourier Transform Infra-red (FTIR) spectroscopy (NICOLET iS50 FT-IR) at 400 to 4000 cm^{-1} wavenumbers were used to determine the surface functional groups of the biosorbent before and after sorption. The surface area of *MOSB* was determined by Brunauer–Emmet–Teller (BET) method using a QuantaChrome NovaWin version 11.03 with nitrogen adsorption-desorption isotherms at 77.35 K. The degassing time was 1 h and the total specific surface area (SSA) was calculated by the multi-point BET method in the lower P/P_0 range of 0.00–0.02.

2.4. Experimental design and statistical data analysis

Five experimental variables (solution contact time: 10–180 min; pH: 2–10; biosorbent dosage: 0.1–2.0 g; temperature: 298 K–338 K; and initial PGT concentration: 20–500 μg L^{-1}) were evaluated based on a central composite design (CCD). To achieve the range of independent input variables, preliminary tests were conducted. The interaction between these variables and their relative significance were studied and optimized collectively by applying RSM. Design Expert Version 13 (Stat-Ease, USA) was used for the experimental planning and statistical analysis of the data. The number of input variables influences the plan matrix. Every parameter has three distinct levels, which are denoted by the numerical values: −1 for low, 0 for center, and +1 for high (Table S1). According to Equation (1), a total of 50 experimental runs were performed (Bayuo et al., 2020):

$$N = 2^n + 2n + n_c \quad \text{(Equation 1)}$$

where n is the number of independent factors, n_c is the number of center points and N is the overall total of experimental runs. 50 experimental runs (Table S2) were used for modeling and optimization and comprised 32 factorial runs, 10 axial runs, and 8 center runs.

The batch biosorption method was used to obtain the dependent parameter (response), which is the percent adsorbed (R), and was employed to generate an empirical mathematical model. Equation (2) is the entire regression equation displaying the interactions between the input parameters (Bayuo et al., 2020).

$$R = b_0 + \sum_{i=1}^{n} b_i X_i + \sum_{i=1}^{n-1} \sum_{j=i+1}^{n} b_{ij} X_i X_j + \sum_{i=1}^{n} b_{ii} X_i^2 \quad \text{(Equation 2)}$$

where R is percent PGT adsorbed; b_0 is the model constant; X_i and X_j are independent variables and b_i, b_{ij}, and b_{ii} are linear coefficients, interaction effect coefficients, and quadratic coefficients, respectively (Bayuo et al., 2020).

2.5. Batch biosorption experiments

The batch experiments were carried out in duplicate by dispersing a CCD-specified biosorbent dosage to a 25 mL solution containing PGT at a known concentration, pH, and temperature according to CCD (Table S3). A detailed methodology is given in Text S3. The amount of adsorbate adsorbed (μg L^{-1}), percentage uptake, and equilibrium biosorption amount (μg g^{-1}) of the PGT were taken as responses. For further analysis and optimization, the percentage removal of PGT (R) was designated as the dependent variable. Equation (3) was used to compute the value of R from aqueous solutions while equation (4) was used to calculate the equilibrium biosorption amount (q_e) (Owino et al., 2023).

$$R = \frac{(C_o - C_e)}{C_o} \times 100\% \quad \text{(Equation 3)}$$

$$q_e = \frac{(C_o - C_e)V}{M} \quad \text{(Equation 4)}$$

where q_e is the equilibrium amount (μg g^{-1}) of PGT adsorbed per gram of *MOSB*, C_o and C_e are the PGT concentrations (μg L^{-1}) in the solution before and after biosorption, respectively. V is the volume (L) of the solution, and M is the mass (g) of the adsorbent.

3. Results and discussion

3.1. Characterization of the biosorbent

3.1.1. Surface chemistry of MOSB

The pH_{pzc} is an index of the surface charge of the biosorbent at different solution pH. The pH_{pzc} of *MOSB* was found to be 6.8 (Fig. S1) implying that *MOSB* surface charge will be positively charged at solution pH levels below 6.8, neutral at solution pH levels of 6.8, and negatively charged at solution pH levels above 6.8 (Bello et al., 2017).

3.1.2. X-ray diffractometry (XRD) analysis of MOSB

The X-ray diffractogram (Fig. 1 (a)) showed weak and unresolved peaks, indicating the predominance of the amorphous nature of the biosorbent, a characteristic that helps the penetration of the adsorbates. This can be attributed to larger quantities of lignin, cellulose, and tannin that give the biosorbent its complex nature (Afolabi et al., 2021; Jayan et al., 2021). For the untreated *MOSB*, there were characteristic peaks at 2θ = 16.47°, 17.3°, 22.47°, and 34.93° which are in agreement with isolated cellulose from *M.O* seeds (Afolabi et al., 2021). For the treated *MOSB,* the peaks at 2θ = 16.47°, and 17.3° were suppressed, those at 2θ = 22.47° and 34.93° were enhanced and there was an additional peak at 27.28° which could be attributed to phosphoric acid hydrolysis.

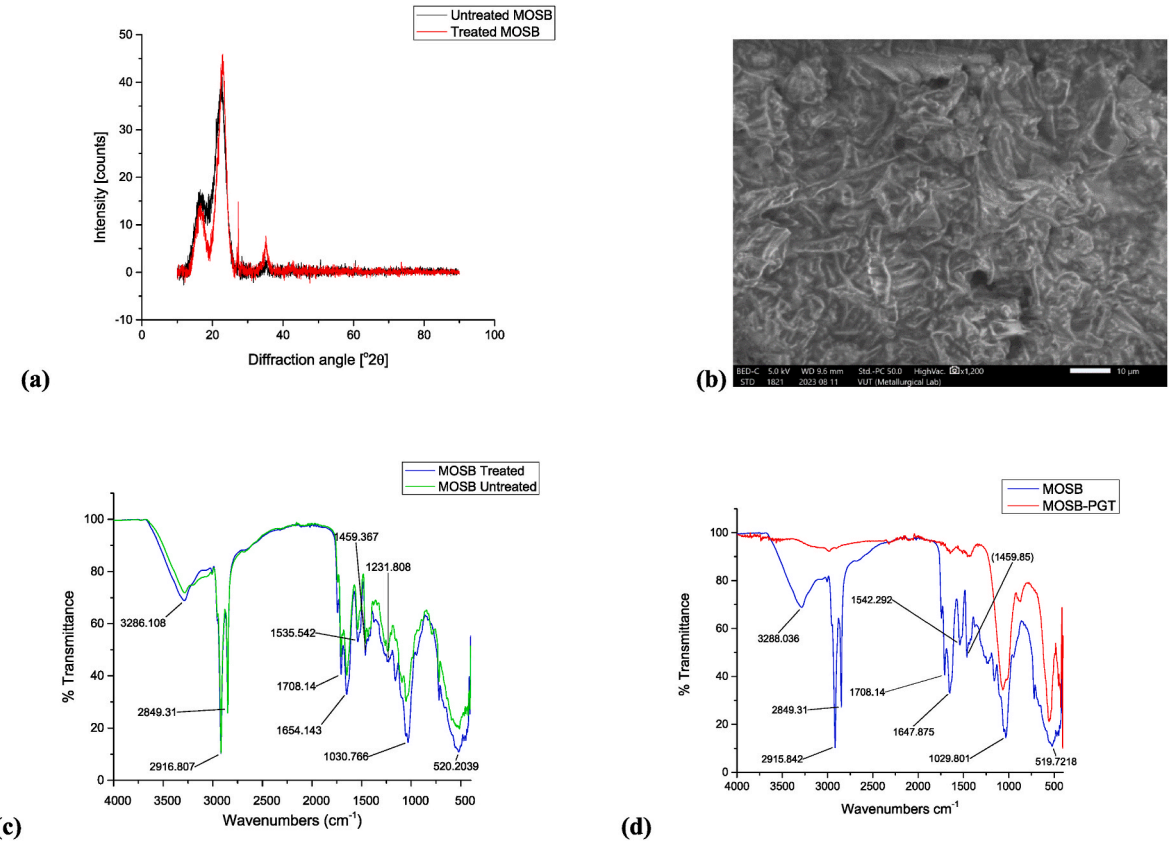

Fig. 1. Characterization analysis (a) X-ray diffractogram for treated and untreated *MOSB* (b) SEM micrograph for treated *MOSB* (c) FT-IR spectra for treated and untreated *MOSB* (d) treated *MOSB* and *MOSB*-PGT.

3.1.3. Scanning electron microscopy - energy-dispersive X-ray spectroscopy (SEM-EDS) analysis

Fig. S2 shows the scanning electron micrographs of the untreated *MOSB* while Fig. 1 (b) displays the micrographs of the treated *MOSB*. The morphology of the treated *MOSB* shows a porous complex fiber matrix with no particular shape, consistent with studies such as Araujo et al. (2010) and Bagheri et al. (2020). After treatment, the phosphate-modified *MOSB* revealed rugged trough-like patterns displaying interstices in the structure that could facilitate the biosorption processes. This gives the material adequate morphological characteristics for retaining PGT.

The major elemental composition of *MOSB* was analyzed by EDS which showed 72.5% carbon and 22.5% oxygen for untreated *MOSB* (Fig. S3 (a)). After treatment, 70.1% of the biomass was found to be carbon while 29.8% was oxygen (Fig. S3 (b)). This is characteristic of carbonaceous materials. The percentage of oxygen is enhanced in the treated *MOSB* due to modification by weak H_3PO_4 which introduced more oxygen. Increased oxygenated functional groups provide more energetically favorable biosorption sites.

3.1.4. Fourier transform infrared spectroscopy (FT-IR) analysis

FT-IR analysis displayed the main functional groups present in *MOSB*. Fig. 1 (c) shows the combined FT-IR spectra for untreated and treated *MOSB*. A general observation from the spectra shows a broad band centered at 3288 cm^{-1} assigned to O–H stretching. This functional group is a major bond in proteins, carbohydrates, fatty acids, lignin units, phenolics and silanols present in *M.O* seeds. Seeds contain a considerable amount of protein, therefore the N–H stretching of amide groups also contributes to this region. The peak at 2916 cm^{-1} is assigned to the asymmetrical stretching of the C–H in the CH_2 group which signifies the existence of methylcellulose. The peak at 2849 cm^{-1} refers to the symmetrical stretching of the C–H bond in the CH_3 group. In the zone between 1800 and 1600 cm^{-1}, there are profound bands attributed to C═O bond stretching and C═C of the aromatic bonds. Fatty acid and protein structures contain the carbonyl group and thus the band at 1708 cm^{-1} is associated with the asymmetrical C═O stretching of the carboxyl found in fatty acids. The band at 1649 cm^{-1} is attributed to the amide group in the protein. The peak at 1541 cm^{-1} is ascribed to C–N stretching or N–H deformation. This band's existence validates the protein structure in *MOSB*. The C–O of carboxylic acids is responsible for the peak at 1460 cm^{-1}, whereas the C–O stretching of carboxylic acids is responsible for the peak at 1238 cm^{-1} (Araujo et al., 2018). After treatment, there was not much shifting of the functional groups nor the creation of new peaks. The intensity of the bands is however enhanced.

After biosorption of PGT (Fig. 1 (d)), the functional groups –OH (3288 cm^{-1}), C–H of CH_2 (2649 cm^{-1}), C–H bond of the CH_3 group (2916 cm^{-1}), C═O bond and C═C (between 1800 and 1600 cm^{-1}), the C–N stretching and/or N–H (1542 cm^{-1}) and the C–O of carboxylic acids (1460 cm^{-1}) were affected. This modification may be connected to the stretching of COO^- bonds present in the heterocyclic ring of PGT. This implies that these groups may be involved in the biosorption of PGT.

3.1.5. Brunauer–Emmet–Teller (BET) analysis

The total specific surface area (SSA) was estimated at 210 $m^2\ g^{-1}$ based on the multi-point BET method. The large SSA further confirmed the favorability of the biosorbent. The linear BET plot (Fig. S4) had a correlation coefficient close to unity ($r = 0.999$) thus yielding accurate values for the SSA.

3.2. Central composite design (CCD) and data analysis

The interaction of the five independent variables, which are initial PGT concentration, biosorbent dosage, pH, temperature, and contact time for the biosorption of PGT to *MOSB* was run based on 50

experiments developed by CCD and the experimental design plan, and the outcomes are represented in Table 1.

The percentage removal depicting the biosorption efficiency of *MOSB* for the abstraction of PGT from aqueous solutions depends on whether the combination of the process parameters shows a significant change. The proposed model for PGT biosorption to *MOSB* was quadratic. ANOVA was used in evaluating the significant variation of the model terms and consequently the adequacy of the proposed model (Table S3).

Based on the F-values and p-values, the proposed model's statistical significance was assessed. The model terms are significant when the p-values (prob > F) are less than 0.05 and vice versa (Jayan et al., 2021). Reduction was carried out to enhance the model because of a few insignificant terms. The reduced quadratic model is shown in Table 2 which displays a **model F-value** of 73.6, which is large enough implying that the model is significant. The linear effects of A (time), B (temperature), D (adsorbate concentration), and E (biosorbent dosage), the interactive effects of AB, AD, AE, BD, BE, CE, and DE, and the quadratic effects of A^2 are significant model terms. C (pH), AC, BC, CD, B^2, C^2, D^2, and E^2 have no significant effect on the biosorption process of PGT. The **lack of fit F-value** of 1.21 suggests that the lack of fit is insignificant in comparison to the pure error and therefore the reduced quadratic model fits. Even after the model reduction, the parameter coded C which was the pH was not significant implying that PGT removal is unaffected by varying pH. This is because PGT is not dissociated under varying pH values, a scenario observed by Moulahcene et al. (2015) and, Banasiak and Schäfer (2010). This means that electrostatic forces probably do not contribute substantially to greater PGT biosorption or that their influence is ignored. The fit statistics gave a regression coefficient (R^2) of 0.964 which was satisfactory. The **predicted R^2** (0.926) was in close consensus with the **adjusted R^2** (0.951) denoting the proposed model is acceptable and reliable.

This reduced quadratic model can be utilized to explore the design space and Equation 5 illustrates the empirical relationship between the five variables involved in the process and biosorption efficiency (R).

Table 1
Results from the experimental design matrix.

Run	Factor 1(A): Time(Mins)	Factor 2 (B): Temperature Kelvin	Factor 3 (C): pH	Factor 4 (D): Adsorbate ppb	Factor 5 (E): Adsorbent g	Response 1: Concentration adsorbed (μg L^{-1})	Response 2: Percentage removal (R)	Response 3: Amount adsorbed (qe) ug g^{-1}
1	180	298	2	20	0.1	17.2 ± 0.04	85.8	4.3
2	10	298	2	20	0.1	16.4 ± 0.05	82.0	4.1
3	10	298	2	500	0.1	441.6 ± 0.65	88.3	110.4
4	95	318	6	260	0.55	233.1 ± 0.07	89.7	10.6
5	180	298	10	500	1	445.6 ± 0.34	89.1	11.1
6	180	298	10	20	0.1	17.3 ± 0.02	86.4	4.3
7	180	338	10	20	0.1	14.2 ± 0.01	71.0	3.5
8	10	338	10	20	1	16.7 ± 0.02	83.5	0.4
9	10	338	10	500	1	445.7 ± 0.01	89.1	11.1
10	95	318	6	260	0.55	231.4 ± 0.02	89.0	10.5
11	180	338	10	20	1	17.8 ± 0.03	89.1	0.4
12	95	298	6	260	0.55	240.7 ± 0.11	92.6	10.9
13	180	338	2	500	1	445.1 ± 0.04	89.0	11.1
14	10	298	10	20	1	16.5 ± 0.01	82.5	0.4
15	95	318	2	260	0.55	232.0 ± 0.01	89.2	10.5
16	10	338	2	500	0.1	423.3 ± 0.10	84.7	105.8
17	95	318	6	260	0.1	226.1 ± 0.08	87.0	56.5
18	10	318	6	260	0.55	218.3 ± 0.03	84.0	9.9
19	95	318	6	20	0.55	17.7 ± 0.05	88.7	0.8
20	95	318	6	260	0.55	229.6 ± 0.06	88.3	10.4
21	180	338	2	20	0.1	14.5 ± 0.01	72.5	3.6
22	95	318	10	260	0.55	232.0 ± 0.04	89.2	10.5
23	10	338	10	500	0.1	424.9 ± 0.03	85.0	106.2
24	180	338	10	500	0.1	383.1 ± 6.06	76.6	95.8
25	10	338	2	20	0.1	14.9 ± 0.03	74.5	3.7
26	95	338	6	260	0.55	230.3 ± 0.05	88.6	10.5
27	10	298	2	500	1	413.1 ± 0.07	82.6	10.3
28	180	338	2	20	1	17.2 ± 0.03	86.0	0.4
29	10	338	2	500	1	435.7 ± 0.10	87.1	10.9
30	10	298	10	500	0.1	437.8 ± 0.03	87.6	109.5
31	180	318	6	260	0.55	216.3 ± 0.05	83.2	9.8
32	180	298	2	20	1	17.8 ± 0.03	89.1	0.4
33	10	338	10	20	0.1	14.2 ± 0.48	71.0	3.5
34	10	338	2	20	1	16.0 ± 0.14	80.0	0.4
35	95	318	6	260	1	235.0 ± 0.35	90.4	5.9
36	10	298	10	20	0.1	16.0 ± 0.16	80.0	4.0
37	180	298	10	20	1	18.0 ± 0.04	90.0	0.5
38	95	318	6	260	0.55	226.4 ± 0.01	87.1	10.3
39	180	338	2	500	0.1	386.2 ± 0.07	77.2	96.5
40	180	338	10	500	1	442.6 ± 0.85	88.5	11.1
41	180	298	2	500	0.1	442.8 ± 0.11	88.6	110.7
42	95	318	6	260	0.55	235.1 ± 0.03	90.4	10.7
43	95	318	6	260	0.55	232.7 ± 0.05	89.5	10.6
44	95	318	6	260	0.55	228.0 ± 0.02	87.7	10.4
45	10	298	10	500	1	416.3 ± 0.01	83.3	10.4
46	180	298	10	500	0.1	441.5 ± 0.43	88.3	110.4
47	10	298	2	20	1	15.5 ± 0.02	77.5	0.4
48	95	318	6	260	0.55	232.0 ± 0.02	89.2	10.5
49	180	298	2	500	1	445.3 ± 0.02	89.1	11.1
50	95	318	6	500	0.55	449.5 ± 0.11	89.9	20.4

Table 2
ANOVA for Reduced Quadratic model.

Source	Sum of Squares	df	Mean Square	F-value	p-value	
Model	1358.90	13	104.53	73.59	<0.0001	significant
A-Time	39.94	1	39.94	28.12	<0.0001	
B-Temperature	140.45	1	140.45	98.88	<0.0001	
C-pH	1.42	1	1.42	1.00	0.3236	
d-Adsorbate	163.05	1	163.05	114.79	<0.0001	
E-Adsorbent	186.32	1	186.32	131.18	<0.0001	
AB	70.25	1	70.25	49.46	<0.0001	
AD	50.26	1	50.26	35.38	<0.0001	
AE	80.99	1	80.99	57.02	<0.0001	
BD	21.38	1	21.38	15.05	0.0004	
BE	218.87	1	218.87	154.09	<0.0001	
CE	15.78	1	15.78	11.11	0.0020	
DE	33.78	1	33.78	23.78	<0.0001	
A^2	336.42	1	336.42	236.86	<0.0001	
Residual	51.13	36	1.42			
Lack of Fit	42.65	29	1.47	1.21	0.4243	not significant
Pure Error	8.48	7	1.21			
Cor Total	1410.04	49				

$$R = 89.15 + 1.08 * A - 2.03 * B + 0.20 * C + 2.19 * D + 2.34 * E - 1.48 * AB - 1.25 * AD + 1.59 * AE + 0.82 * BD + 2.62 * BE + 0.70 * CE - 1.03 * DE - 5.56 * A^2 \quad \text{(Equation 5)}$$

where A-E are the coded values for the independent variables, and R is the percentage removal indicating biosorption efficiency. Coefficients featuring a single factor demonstrate the influence of that specific component, whereas coefficients containing multiple variables describe the interaction of those variables. Synergistic effects are indicated by a positive sign before the terms, and antagonistic effects are indicated by a negative sign (Ani et al., 2019). For specific levels of each coded factor, Equation (5) can be applied in computing the response. The high values of the factors are coded as +1, while the low levels are coded as −1. By comparing the factor coefficients, Equation (5) can be used to determine the significance of the process variables. Fig. 2 (a), a graph of actual experimental values versus predicted values, displays a reasonable distribution along a straight line implying a good relationship. Diagnostic plots providing additional information about the model's fitness by correlating the experimental and predicted values of biosorption of PGT to *MOSB* are shown in Fig. 2(b–d). Fig. 2 (b) displays a straight line when the normal percentage probability is plotted against internally

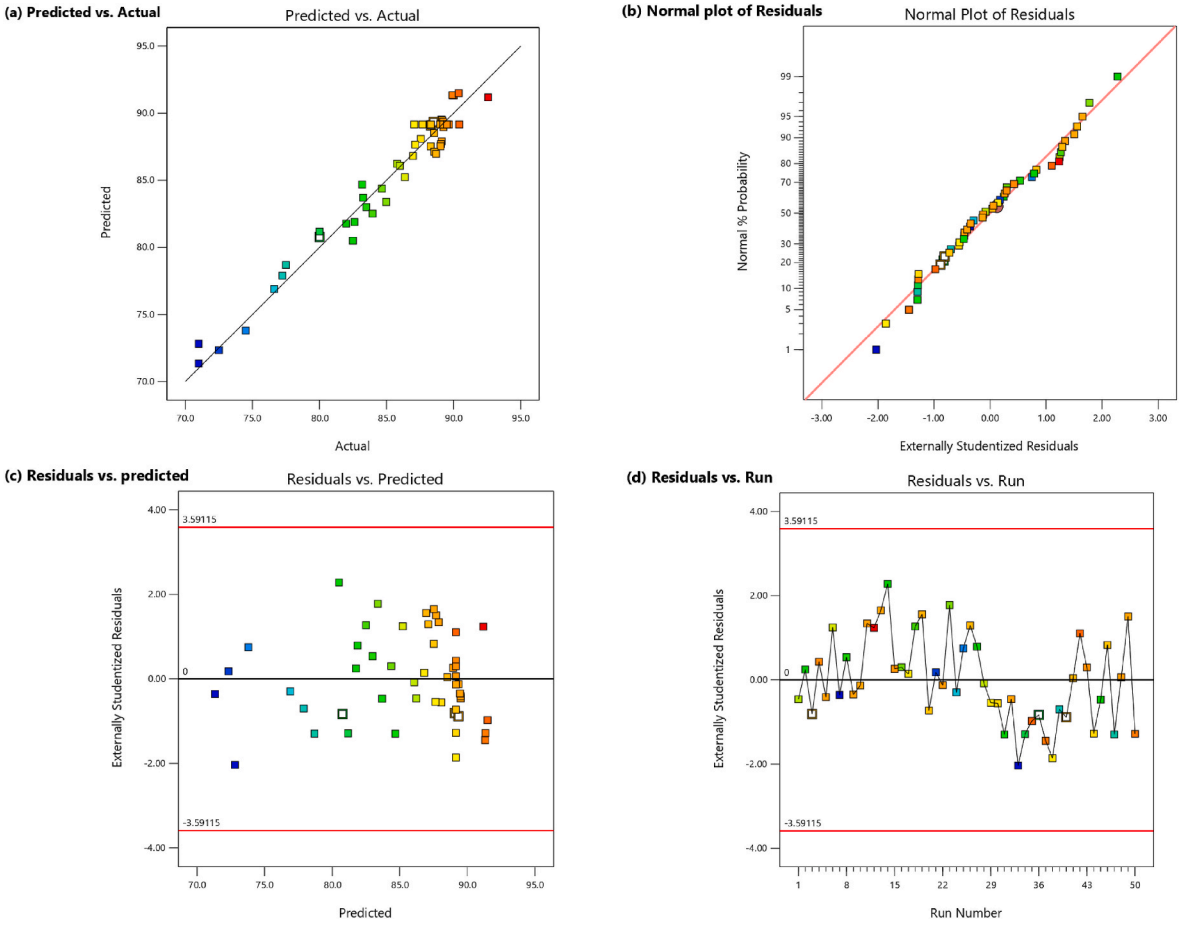

Fig. 2. Diagnostic plots: (a) Actual experimental values versus predicted values (b) Normal plot of residuals (c) Residuals vs. predicted (d) Residuals vs. run.

studentized residuals demonstrating that the error terms have a normal distribution. This validated the goodness of fit of the model predictions. In Fig. 2 (c), the random scatter along a center line of the residuals of the predicted values of PGT biosorption illustrates that the observed and predicted values agree, and this is corroborated by Fig. 2 (d) showing a distribution along a center line in the residuals of the run. The Box-Cox plot (Fig. S5 (b)) for power transform did not recommend any data transformation.

3.3. Model graphs for all factor interactions

Fig. S6 (a) displays all factor perturbation around a reference point of contact time-95 min, temperature-318 K, adsorbate concentration of 260 μg L^{-1}, pH-6, and 0.55g of biosorbent. Fig. S6 (b-f) shows the impact of independent parameters on the biosorption process, taking into consideration all the factor interactions. As contact time varied from 10 to 180 min, there was a faster initial increase reaching a peak before a decrease in percentage removal (Fig. S6(b)) due to abundant vacant pores before saturation and equilibrium is achieved (Luttah et al., 2023). The removal efficiency dropped as the temperature increased from 298 to 338 K (Fig. S6(c)). Fig. S6(d) corroborates the ANOVA tests displaying PGT removal being unaffected by pH and the percentage removal remaining practically constant. As the concentration of PGT rose, the percentage eliminated increased alongside the quantity adsorbed, as seen in Fig. S6(e). The amount adsorbed rose from 87.3% to 90.4% as the amount of *MOSB* was increased from 0.1 to 1 g (Fig. S6(f)). This corresponds to the rising vacant pores (Aly-Eldeen et al., 2018). When the biosorbent-to-adsorbate concentration ratio is larger, there is swift surface sorption onto the biosorbent, resulting in a lower adsorbate concentration in the solution than when the biosorbent-to-adsorbate concentration ratio is smaller. This is because a specific amount of biosorbent with a fixed number of available binding sites can only adsorb a particular quantity of PGT. Consequently, the higher the biosorbent dose, the greater the concentration of PGT purified by a certain amount of *MOSB*.

3.4. Three-dimensional surface plots for the biosorption of PGT onto MOSB

To estimate the impact of the various interactions of independent factors on biosorption efficiency, three-dimensional (3-D) response surface plots were generated. The 3-D plots are shown in Fig. 3(a–f) and their respective contour plots giving more visual representation of the observations are in the supplementary information (Fig. S7 (a-f)). From Fig. 3 (a), biosorption efficiency was affected by both contact time and temperature. Closer to room temperature (298 K), suitable for real wastewater treatment, was more favorable. The optimal area of efficiency was observed between 74 min and 163 min and thereafter there was a decrease depicting desorption. The same range of contact time and increased amount of adsorbate and biosorbent augmented the biosorption efficiency (Fig. 3 (b & c)). Furthermore, lower temperature and increased initial concentration of PGT and biosorbent dosage improved the percentage removal (Fig. 3 (d)). In addition, at higher values of initial PGT concentration and biosorbent dosage, the collective effect was greater (Fig. 3 (e)).

3.5. Optimization of the biosorption process

In the optimization analysis, the dependent variables, percentage removal and amount adsorbed (q_e), were set at maximum. For the independent factors, the temperature was minimized to depict experiments carried out at room temperature, and the pH was targeted at 7 to depict near-natural conditions of wastewater treatment; the biosorbent was minimized to ease disposal after use; the adsorbate was maximized while the contact time was left in range. The goal was to find the best settings that would result in the best response. Based on the desirability function, the optimum response in terms of percentage removal was found to be 93.7% and 109 μg g^{-1} amount adsorbed at a contact time of

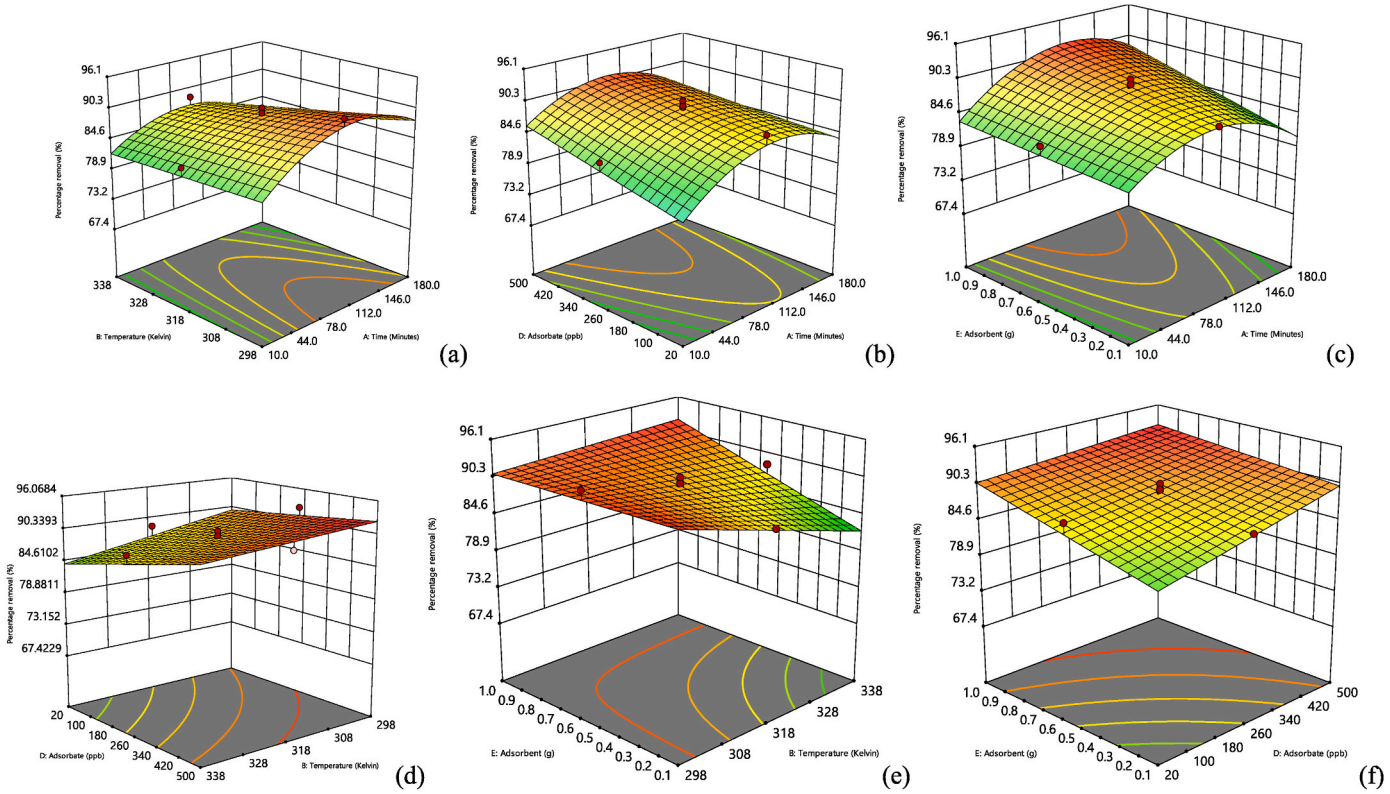

Fig. 3. (a–f): 3-D plots estimating the effect of the combinations of the independent variables on the adsorption efficiency.

86.8 min, pH of 7.0, a temperature of 298 K, biosorbent dosage of 0.1 g and a desirability function of 0.995. The ramps displaying the optimized parameters are shown in Fig. S8 in the supplementary file. This confirms the validity of the proposed quadratic model and reliability in predicting the response (R). Acid-activated *MOSB* has been demonstrated to be an inexpensive alternative biosorbent capable of abstracting PGT from aqueous media.

3.6. Biosorption isotherm studies

To obtain the biosorption isotherms, the initial PGT concentration (20–500 μgL^{-1}) was varied as all the parameters were kept constant at the optimized parameters (pH-7; contact time-87 min; biosorbent dosage of 0.1 g and 298 K). Following equilibration, the remaining PGT in the solution was determined, and the equilibrium biosorption capacity, *qe*, at various initial PGT concentrations, was calculated using Equation (6) (Owino et al., 2023).

$$q_e = \frac{(C_{o-} C_e)V}{M} \quad \text{(Equation 6)}$$

Higher adsorbate concentrations resulted in the rise of both the percentage removed and the amount adsorbed. This implies that more molecules of the adsorbate are being taken up by the vacant pores of the biosorbent. This is because increased concentration levels offer an intense impetus of the concentration gradient, which aids in overcoming the mass transfer resistance of the PGT molecules between the liquid and solid phases (Aly-Eldeen et al., 2018; Bayuo et al., 2020).

The experimental data were fitted to two-parameter isotherm models, namely, Langmuir and Freundlich, and three-parameter isotherm models, namely, Redlich–Peterson and Sips. The Redlich–Peterson model (Equation (7)) (Redlich and Peterson, 1959) combines Langmuir and Freundlich models and if data fits the model, then the biosorption is hybrid implying that ideal monolayer sorption is not feasible. Due to its versatility, it applies to homogeneous or heterogeneous surfaces.

$$q_e = \frac{AC_e}{1 + BC_e^g} \quad \text{(Equation 7)}$$

where C_e denotes the equilibrium concentration of the solute (μg/L), q_e represents equilibrium biosorption capacity (μg g^{-1}), A (L μg^{-1}), B (L g^{-1}) denotes the constants of the Redlich–Peterson model and g represents an exponent expressing the heterogeneity of the biosorbent and its values between 0 and 1. When g values are equal to zero and one, the Redlich-Peterson isotherm converges to the Henry and Langmuir isotherms, respectively. Furthermore, when the isotherm parameters A and $B \gg 1$ and $g < 1$, the Redlich–Peterson isotherm will represent the Freundlich isotherm (Equations (8) and (9)) which is possible at high solute concentration in the liquid phase.

$$q_e = \frac{A}{B} C_e^{(1-g)} \quad \text{(Equation 8)}$$

where $A/B = K_F$ and $(1-g) = 1/n$ of the Freundlich model translating to:

$$q_e = K_f C_e^{\frac{1}{n}} \quad \text{(Equation 9)}$$

Equation (7) changes to the Langmuir isotherm (Equation (10)) when g = 1 and with b = B [Langmuir constant (L g^{-1}), which is associated with the biosorption energy]. $A = bq_m$ and q_m represent Langmuir's maximum biosorption capacity of the biosorbent (μg g^{-1}). (Freundlich, 1906).

$$q_e = \frac{q_{max} C_e}{1 + K_L C_e} \quad \text{(Equation 10)}$$

Where q_e (μg g^{-1}) and C_e (μg L^{-1}) are the adsorbed solute and the solution concentration at equilibrium, respectively, and Q_o (μg g^{-1}) is the monolayer biosorption capacity. C_o (μg L^{-1}) is the initial solution concentration. The K_L (L mg^{-1}) and K_f (L g^{-1}) are the Langmuir and Freundlich constants and 1/n is the biosorption affinity or surface heterogeneity index (Langmuir, 1916).

When β = 0, equation (7) becomes Henry's model having A/B as Henry's constant (K_{HE}).

$$q_e = K_{He} Ce \quad \text{(Equation 11)}$$

In heterogeneous biosorption, where the adsorbed molecule has numerous biosorption sites, the Sips isotherm (Equation (12)), which combines the Freundlich and Langmuir isotherms is the most appropriate (Sips, 1948). Adsorbate-adsorbate synergy, however, is not considered by the model.

$$q_e = \frac{q_{MS} a_s C_e^{B_s}}{1 + a_s C_e^{B_s}} \quad \text{(Equation12)}$$

Where q_{ms}, a_s, and B_s are the isotherm constants. The constant B_s is the heterogeneity index whose magnitude increases with heterogeneity.

The isotherms plots are represented in Fig. 4 (a) and Table 3 (a) highlights the biosorption isotherm parameters. The Langmuir model was able to adequately describe the experimental sorption data as depicted by the R^2 and the chi-square values (Table 3 (a)) thus implying a monolayer; however, other biosorption surfaces were also available and contributed to the biosorption process, hence, the description by Sips model (Bagheri et al., 2020). This agrees with the Redlich-Peterson isotherm model whose g value was unity implying a leaning towards the Langmuir isotherm model. This is further corroborated by the Sips model where when the B_s value is closest to unity (0.950), it suggests a monolayer type of biosorption which is consistent with the Langmuir equation (Shikuku and Jemutai-Kimosop, 2020). The sips model closely followed the Langmuir model predicting a maximum biosorption capacity of 139.94 μg g^{-1}. In summary, the equilibrium data fitted the isotherms in the following order: Langmuir > Sips > Redlich-Peterson > Freundlich. All the isotherms gave an $R^2 > 0.94$ thus implying that the biosorption was multi-mechanistic. From the Freundlich parameters, according to Treybal (1981), the value of n demonstrates the favorability of the biosorption process. Accordingly, n values in the range 2–10 represent favorable, 1–2 moderately unfavorable, and less than 1 a poor adsorptive potential. In this study, the magnitude of n (2.54) signifies a favorable biosorption process. Furthermore, 1/n indicates the strength of the adsorbate-biosorbent bonds. A value less than 1 indicates weak adsorbate-biosorbent interaction indicating physisorption. The value obtained in this study (0.394) therefore implies that the process was physisorption and the interactions were weak (Shikuku and Jemutai-Kimosop, 2020).

Giles et al. (1974) categorized organic solute biosorption into four depending on their shapes: L, S, H, and C, and subsequently into subgroups. According to this sub-division, the isotherm of PGT biosorption displayed an L-type curve, subgroup 2c. In L-type curves, also called type 1 or normal curves, the L stands for Langmuir which in essence is consistent with data in this study fitting more into the Langmuir model. In such kinds of curves, the slope usually falls with a rise in adsorbate concentration because all biosorption sites are occupied. The subgroup (2c) is majorly displayed by a microporous substrate, further confirming the porosity of *MOSB*.

3.7. Kinetic studies

Having optimized the parameters required (pH-7; initial PGT concentration-500 μg L^{-1}; biosorbent dosage of 0.1 g and 298 K), the biosorption kinetics experiments were performed by varying the contact time (0–180 min). Equation (13) was used to determine how much PGT was adsorbed per unit mass at time (t).

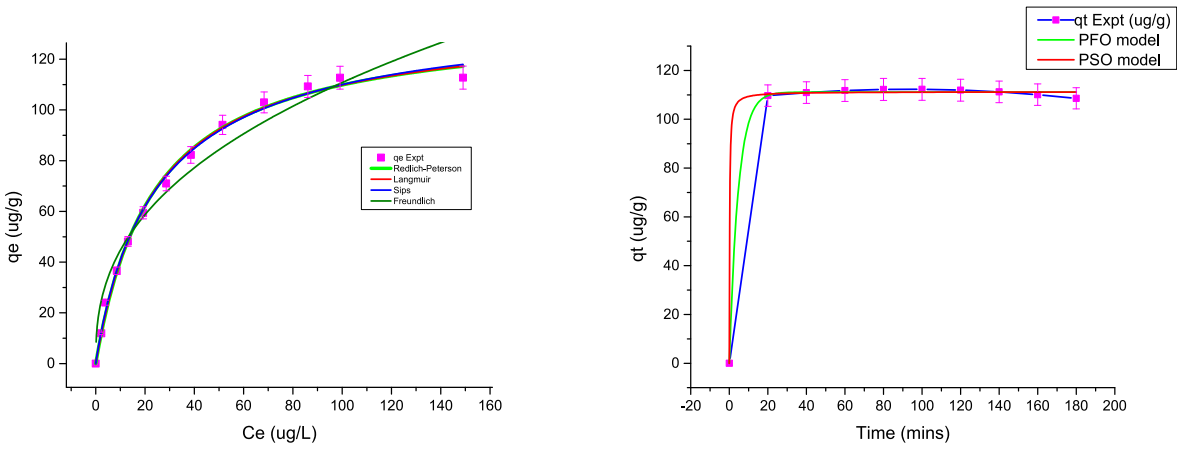

Fig. 4. (a) Adsorption isotherms (b) Kinetic model graphs for PGT biosorption to *MOSB*.

Table 3
(a) - Adsorption isotherm parameters, (b) - Calculated kinetic parameters for PGT biosorption to *MOSB*, (c) - Thermodynamic parameters for PGT adsorption onto *MOSB*.

(a)				
Isotherm	Langmuir	Freundlich	Redlich-Peterson	Sips
Parameters	Q_{max} = 135.848 K_L = 0.042	1/n = 0.394 K_F = 18.025	A = 5.742 B = 0.042 g = 1	a_s = 0.046 q_{MS} = 139.938 B_s = 0.950
Coefficient of determination (R^2)	0.995	0.942	0.995	0.995
Chi-square (χ^2)	7.706	75.038	8.476	8.092

(b)		
Kinetic model	PFO	PSO
Parameters	q_e (cal) (μg g^{-1}) = 111.146 k_1 (min^{-1}) = 0.217 q_e (expt) (μg g^{-1}) = 111.1	q_e (cal) (μg g^{-1}) = 111.289 k_2 (min^{-1}) = 0.051 q_e (expt) (μg g^{-1}) = 111.1
S_{rate} (μg g^{-1} min^{-1})	24.119	631.647
$t_{1/2}$ (min^{-1})	3.194	0.176
R^2	0.99887	0.99874
χ^2	1.39884	1.55385

(c)				
	% removal	ΔG (kJ mol^{-1})	ΔH (kJ mol^{-1})	ΔS (J mol^{-1})
298	89.83	−22.51	−9.258	+44.16
308	88.03	−22.80		
318	86.62	−23.20		
328	85.62	−23.70		
338	85.02	−24.29		

$$q_t = \frac{(C_o - C_t)V}{M} \quad \text{(Equation 13)}$$

Where C_o and C_t are the initial and equilibrium concentration (μg L^{-1}), M is the biosorbent mass (g) and V is the volume of the solution (L).

There was a faster initial uptake reaching a peak before a decrease in percentage removal. PGT's initial rapid biosorption was facilitated by the abundance of vacant binding sites as confirmed by the initial biosorption rate (Sr_{ate}) and the half-life ($t_{1/2}$). There was no discernible change in the amount in the solid phase depicting achieved equilibrium as time passed. The equilibrium changed towards desorption as a result of saturation of the binding sites, repulsion between adsorbed PGT and those in bulk solution, and inaccessibility of the active inner pore sites.

The kinetic data was fitted to two frequently used kinetic models, namely, pseudo-first-order (PFO) (Ho and McKay, 1998), and pseudo-second-order (PSO) (Ho, 2006) represented in Equations (14) and (15), respectively:

$$\text{Pseudo} - \text{first} - \text{order model}: q_t = q_e\left(1 - e^{k_1 t}\right) \quad \text{(Equation 14)}$$

$$\text{Pseudo} - \text{second} - \text{order model}: q_t = \frac{q_e^2 k_2 t}{1 + k_2 q_e t} \quad \text{(Equation 15)}$$

Where t (min) and q_t (μg g^{-1}) are time and amount adsorbed at equilibrium time, respectively, while q_e is the equilibrium biosorption capacity. k_1 (min^{-1}) and k_2 (g μg^{-1} min^{-1}) are rate constants. Assuming PFO kinetics, the initial biosorption rate (S_{rate}) and biosorption half-life ($t_{1/2}$) were evaluated using Equations (16) and (17), respectively.

$$S_{rate} = K_1 q_e \quad \text{(Equation 16)}$$

$$t_{1/2} = \frac{ln\,2}{K_1} \quad \text{(Equation 17)}$$

Equations (18) and (19) were used to calculate the initial sorption rate and biosorption half-life for PSO.

$$S_{rate} = K_2 q_e^2 \quad \text{(Equation 18)}$$

$$t_{1/2} = \frac{1}{K_2 q_e} \quad \text{(Equation 19)}$$

The comparative fitting of the experimental data to the kinetic models is shown in Fig. 4 (b). The model's suitability to represent reaction kinetics was determined based on the proximity between experimental (q_{exp}) and model-predicted (q_{cal}) equilibrium biosorption capacities and the R^2 and χ^2 values. The calculated kinetic models' parameters are presented in Table 3 (b). Based on the R^2 and χ^2, and the closeness between the experimental (q_{exp}) and the model-predicted (q_{cal}) equilibrium biosorption capacities, both the pseudo-first-order (PFO) and pseudo-second-order (PSO) model forecasted the biosorption kinetics comparatively well but PFO gave the best fit. The PFO model assumes a physisorption-governed rate-determining step.

3.8. Biosorption thermodynamics

Over a temperature range of 298–338 K, the impact of temperature changes on biosorption was investigated. Here, 25 mL of 500 g L^{-1} of PGT at pH 7, was added to 0.1 g of *MOSB* and swirled using a temperature-controlled magnetic stirrer at various temperatures (298, 308, 318, 328 and 338 K), until equilibration at 87 min. Using equations (20)–(22), the thermodynamic parameter, change in Gibbs free energy (ΔG) was calculated.

$$\Delta G = -RTlnK_c \quad \text{(Equation 20)}$$

$$K_c = 1000K_d \quad \text{(Equation 21)}$$

$$K_d = \frac{C_{ads}}{C_e} \quad \text{(Equation 22)}$$

Where K_c is the equilibrium constant (dimensionless), C_{ads} is the equilibrium solid phase concentration (μg L^{-1}) and C_e is the solution's equilibrium concentration (μg L^{-1}). T is the temperature in Kelvin and R is the gas constant (8.314 J mol^{-1} K^{-1}). K_d is the distribution coefficient (L g^{-1}), and the density of water is 1000 g L^{-1} (Luttah et al., 2023). The changes in entropy (ΔS) (J mol^{-1}) and enthalpy (ΔH) (kJ mol^{-1}) were obtained from the intercept and slope of the Van't Hoff plot (Equation (23)), respectively (Shikuku et al., 2015).

$$\ln K_c = \frac{\Delta s}{R} - \frac{\Delta H}{R}\frac{1}{T} \quad \text{(Equation 23)}$$

From Table 3 (c), there was a reduction in the percent removal of PGT with every increase in temperature implying an exothermic process. This is confirmed by the negative ΔH value (−9.258 kJ mol^{-1}). The decline is caused by greater water solubility at elevated temperatures by most adsorbates, adsorbate's reduced attraction for the biosorbent surface (Jemutai-Kimosop et al., 2020), and the exothermicity of the reaction which makes it less favorable with increased temperature. The biosorption of PGT to *MOSB* can thus be carried out at room temperature thus suiting utilization in real wastewater treatment systems. The ΔH value (−9.258 kJ mol^{-1}), far below the standard range of 40–120 kJ mol^{-1} for the chemisorption mechanism, implies that the biosorption mechanism of PGT onto *MOSB* is physical with no exchange in electrons, thus consistent with the PFO model. The negative ΔG values imply that the biosorption of PGT onto *MOSB* is a spontaneous and favorable process. The physical biosorption mechanism suggested previously is supported by the comparatively small magnitudes of ΔG values. Further confirming exothermicity, the magnitude of ΔG increased with an increase in temperature thus becoming less favorable. The enhanced disorderliness and affinity of the biosorbent for the adsorbate at the liquid-solid interface has been demonstrated by the positive ΔS value (Luttah et al., 2023).

3.9. Effect of pH

Solution pH, the surface charge of the biosorbent, and the pKa values of the adsorbate are variables that determine the mechanism of biosorption which could be a complex interplay between electrostatic, non-electrostatic, and hydrophobic interactions (Ngeno et al., 2016). Over a pH range of 2–12, the impact of pH on the amount of PGT elimination was examined. The percent removal as a function of pH is displayed in Fig. S9 pH variations did not greatly affect PGT biosorption, with percent removal ranging from 89.8 to 90.1% in the chosen pH range. The surface charge of the biosorbent (pH_{zpc}) (Fig. S1) was 6.8 (neutral) and the surface charge of the biosorbent is predicted to be positive below this number and negatively charged above it. 44% of *M.O* seeds are proteins of which 53% are globulins and 44% are albumins. These water-soluble proteins in *M.O* have a net positive charge (Militao et al., 2022). However, during modification with H_3PO_4, negatively charged phosphates from dissociated H_3PO_4 interact with the positively charged *MOSB* resulting in a neutral species (Fig. S10) (Bagheri et al., 2020) thus confirming the neutrality of the biosorbent surface. Focusing on PGT, it is characterized by two pKa values; pKa_1 at −4.8 and pKa_2 at 18.92. Therefore, in the pH range of 2–12 of the study, PGT existed entirely as a neutral species implying that PGT is undissociated under varying pH conditions. As a result, electrostatic attractions were deemed negligible and consequently ruled out as a biosorption mechanism since both the biosorbent and adsorbate are neutral species unaffected by changes in pH. This is supported by similar observations by Moulahcene et al. (2015) as well as the independence of the % removal from solution pH. The mechanism of biosorption could be ascribed to π-π interactions facilitated by the availability of oxygen-containing functional groups such as carbonyl in PGT interacting with aromatic rings (π electron receptors) found in the carbonaceous biomass compounds, such as lignin, cellulose, and hemicellulose (Araujo et al., 2018). Furthermore, its Log K_{ow} of 3.87 and water solubility of 8.81 mg L^{-1} at 25 °C make it hydrophobic (National Centre for Biotechnology Information, 2022). Consequently, the interaction between the PGT's hydrophobic chain with the hydrophobic regions of *MOSB* contributes to the biosorption mechanism.

3.10. Comparison of MOSB with other adsorbents in the removal of PGT and other pollutants

The sequestration of different pollutants using *M.O* biosorbents was compared and is shown in Table S4.

3.11. Study strengths, limitations and recommendations

To the best of our knowledge, this is the first time acid-activated, fat-free *M.O* seeds are being investigated for the removal of PGT from aqueous solutions with RSM as an experimental design tool for the optimization of process parameters. Nonetheless, there were some study limitations encountered; firstly, due to the inadequacy of facilities, the biosorbent was not characterized using X-ray photoelectron spectroscopy (XPS). This was however countered by carrying out SEM-EDS which equally gave the elemental composition. Secondly, biosorption in real wastewater and regeneration of the biosorbent were outside the scope of the study and future prospective studies may wish to explore these areas.

4. Conclusions

In this work, acid-activated fat-free *MOSB* was used for the biosorption of PGT from aqueous solution using CCD for the optimization of process parameters. Based on RSM, the optimized parameters, displaying a 93.7% removal efficiency were 86.8 min contact time, 298 K, 500 μg L^{-1} as initial adsorbate concentration, and a 0.1 g biosorbent. Biosorption efficiency was unaffected by pH variation. The equilibrium biosorption data were best described by the Langmuir model with an estimated maximum biosorption capacity of 135.8 μg g^{-1}. Biosorption kinetics followed pseudo-first-order (PFO) kinetics while thermodynamics investigation revealed the biosorption process to be spontaneous ($\Delta G < 0$), exothermic ($\Delta H = -9.258$ kJ mol^{-1}), and random ($\Delta S = +44.16$ J mol^{-1}). The magnitude of ΔH and conformity to PFO indicated that the biosorption mechanism was physical.

CRediT authorship contribution statement

Emily Ngeno: Conceptualization, Formal analysis, Investigation, Methodology, Writing – original draft. **Roselyn Ongulu:** Conceptualization, Supervision, Writing – review & editing. **Victor Shikuku:** Writing – review & editing. **Deo Ssentongo:** Methodology, Writing – review & editing. **Benton Otieno:** Methodology, Writing – review & editing. **Patrick Ssebugere:** Conceptualization, Funding acquisition, Project administration, Supervision, Writing – review & editing. **Francis Orata:** Conceptualization, Funding acquisition, Supervision, Writing – review & editing.

Declaration of competing interest

The authors declare that they have no known competing financial interests or personal relationships that could have appeared to influence the work reported in this paper.

Data availability

Data will be made available on request.

Acknowledgments

This study was supported by the Organization for Women Scientists for the Developing World (OWSD), Kenya National Research Fund (NRF), International Foundation for Science (1I2_W_042583_REV), Mawazo, AGNES-PAWS, Makerere University Research and Innovation Fund (MAKRIF/CH/01/21) and APPEAR Academic Partnership (Project 249). Patrick Ssebugere acknowledges the Alexander von Humboldt Foundation for the financial support during his 12-month research fellowship at Helmholtz Centre for Environmental Research-UFZ, Germany (UGA-1185413-GF-E).

Appendix A. Supplementary data

Supplementary data to this article can be found online at https://doi.org/10.1016/j.chemosphere.2024.142457.

References

Afolabi, A., Oluyamo, S., Fuwape, I., 2021. Synthetic characterization and structural properties of Nanocellulose from Moringa oleifera seeds. Journal of the Nigerian Society of Physical Sciences 3, 148–153.

Ahalya, N., Kanamadi, R.D., Ramachandra, T.V., 2006. Biosorption of iron(III) from aqueous solutions using the husk of Cicer arientinum. Indian J. Chem. Technol. 13, 122–127.

Almazrouei, B., Islayem, D., Alskafi, F., Catacutan, M.K., Amna, R., Nasrat, S., Yildiz, I., 2023. Steroid hormones in wastewater: Sources, treatments, environmental risks, and regulations. Emerging Contam. 9, 100210.

Aly-Eldeen, M.A., El-Sayed, A.A., Salem, D.M., El Zokm, G.M., 2018. The uptake of Eriochrome Black T dye from aqueous solutions utilizing waste activated sludge: adsorption process optimization using factorial design. The Egyptian Journal of Aquatic Research 44, 179–186.

Ani, J., Okoro, U., Aneke, L., Onukwuli, O., Obi, I., Akpomie, K., Ofomatah, A., 2019. Application of response surface methodology for optimization of dissolved solids adsorption by activated coal. Appl. Water Sci. 9, 1–11.

Anwar, F., Latif, S., Ashraf, M., Gilani, A.H., 2007. Moringa oleifera: a food plant with multiple medicinal uses. Phytotherapy Research: An International Journal Devoted to Pharmacological and Toxicological Evaluation of Natural Product Derivatives 21 (1), 17–25.

Araujo, C.S., Alves, V.N., Rezende, H.C., Almeida, I.L., de Assuncao, R.M., Tarley, C.R., Coelho, N.M.M., 2010. Characterization and use of *Moringa oleifera* seeds as biosorbent for removing metal ions from aqueous effluents. Water Sci. Technol. 62, 2198–2203.

Araujo, L.A., Bezerra, C.O., Cusioli, L.F., Silva, M.F., Nishi, L., Gomes, R.G., Bergamasco, R., 2018. *Moringa oleifera* biomass residue for the removal of pharmaceuticals from water. J. Environ. Chem. Eng. 6, 7192–7199.

Bagheri, A., Abu-Danso, E., Iqbal, J., Bhatnagar, A., 2020. Modified biochar from Moringa seed powder for the removal of diclofenac from aqueous solution. Environ. Sci. Pollut. Control Ser. 27, 7318–7327.

Banasiak, L.J., Schäfer, A.I., 2010. Sorption of steroidal hormones by electrodialysis membranes. J. Membr. Sci. 365, 198–205.

Bayuo, J., Abukari, M.A., Pelig-Ba, K.B., 2020. Optimization using central composite design (CCD) of response surface methodology (RSM) for biosorption of hexavalent chromium from aqueous media. Appl. Water Sci. 10, 1–12.

Bello, O.S., Lasisi, B.M., Adigun, O.J., Ephraim, V., 2017. Scavenging Rhodamine B dye using *Moringa oleifera* seed pod. Chem. Speciat. Bioavailab. 29, 120–134.

Chang, H., Wan, Y., Wu, S., Fan, Z., Hu, J., 2011. Occurrence of androgens and progestogens in wastewater treatment plants and receiving river waters: comparison to estrogens. Water Res. 45, 732–740.

Chimi, T., Hannah, B.U., Lincold, N.M., Jacques, M.B., Tome, S., Hermann, D.T., Meva, F. E.a., 2023. Preparation, characterization and application of H3PO4-activated carbon from Pentaclethra macrophylla pods for the removal of Cr(VI) in aqueous medium. J. Iran. Chem. Soc. 20, 399–413. https://doi.org/10.1007/s13738-022-02675-9.

Freundlich, H., 1906. Over the adsorption in solution. J. Phys. chem 57, 1100–1107.

Ghasemi, A., Khansary, M.A., Marjani, A., Shirazian, S., 2017. Using quantum chemical modeling and calculations for evaluation of cellulose potential for estrogen micropollutants removal from water effluents. Chemosphere 178, 411–423.

Giles, C.H., Smith, D., Huitson, A., 1974. A general treatment and classification of the solute adsorption isotherm. I. Theoretical. J. Colloid Interface Sci. 47, 755–765.

Golovko, O., Šauer, P., Fedorova, G., Kroupová, H.K., Grabic, R., 2018. Determination of progestogens in surface and wastewater using SPE extraction and LC-APCI/APPI-HRPS. Sci. Total Environ. 621, 1066–1073.

Grosshagauer, S., Pirkwieser, P., Kraemer, K., Somoza, V., 2021. The future of Moringa foods: a food chemistry perspective. Front. Nutr. 8, 751076.

Ho, Y.-S., 2006. Review of second-order models for adsorption systems. J. Hazard Mater. 136, 681–689.

Ho, Y.-S., McKay, G., 1998. Sorption of dye from aqueous solution by peat. Chem. Eng. J. 70, 115–124.

Ifelebuegu, A., Ukpebor, J., Nzeribe-Nwedo, B., 2016. Mechanistic evaluation and reaction pathway of UV photo-assisted Fenton-like degradation of progesterone in water and wastewater. Int. J. Environ. Sci. Technol. 13, 2757–2766.

Imran, M., Anwar, K., Akram, M., Shah, G.M., Ahmad, I., Samad Shah, N., Ahmad, S., 2019. Biosorption of Pb (II) from contaminated water onto Moringa oleifera biomass: kinetics and equilibrium studies. Int. J. Phytoremediation 21, 777–789.

Jayan, N., Bhatlu M, L.D., Akbar, S.T., 2021. Central composite design for adsorption of Pb (II) and Zn (II) metals on PKM-2 *Moringa oleifera* leaves. ACS Omega 6, 25277–25298.

Jemutai-Kimosop, S., Orata, F., Shikuku, V.O., Okello, V.A., Getenga, Z.M., 2020. Insights on adsorption of carbamazepine onto iron oxide modified diatomaceous earth: kinetics, isotherms, thermodynamics, and mechanisms. Environ. Res. 180, 108898.

Kasonga, T.K., Coetzee, M.A., Kamika, I., Ngole-Jeme, V.M., Momba, M.N.B., 2021. Endocrine-disruptive chemicals as contaminants of emerging concern in wastewater and surface water: a review. J. Environ. Manag. 277, 111485.

Keereerak, A., Chinpa, W., 2020. A potential biosorbent from *Moringa oleifera* pod husk for crystal violet adsorption: kinetics, isotherms, thermodynamic and desorption studies. Sci. Asia 46, 186–194.

Korde, S., Deshmukh, S., Tandekar, S., Jugade, R., 2021. Implementation of response surface methodology in physi-chemisorption of Indigo carmine dye using modified chitosan composite. Carbohydrate Polymer Technologies and Applications 2, 100081.

Langmuir, I., 1916. The constitution and fundamental properties of solids and liquids. Part I. Solids. J. Am. Chem. Soc. 38, 2221–2295.

Luttah, I., Onunga, D.O., Shikuku, V.O., Otieno, B., Kowenje, C.O., 2023. Removal of endosulfan from water by municipal waste incineration fly ash-based geopolymers: adsorption kinetics, isotherms, and thermodynamics. Frontiers in Environmental Chemistry 4, 1164372.

Maina, I.W., Obuseng, V., Nareetsile, F., 2016. Use of *Moringa oleifera* (Moringa) seed pods and Sclerocarya birrea (Morula) nut shells for removal of heavy metals from wastewater and borehole water. J. Chem. 2016, 9312952.

Militao, I.M., Roddick, F., Bergamasco, R., Fan, L., 2022. Rapid adsorption of PFAS: application of *Moringa oleifera* seed powder encapsulated in alginate beads. Environmental Technology & Innovation 28, 102761.

Moulahcene, L., Skiba, M., Senhadji, O., Milon, N., Benamor, M., Lahiani-Skiba, M., 2015. Inclusion and removal of pharmaceutical residues from aqueous solution using water-insoluble cyclodextrin polymers. Chem. Eng. Res. Des. 97, 145–158.

Mukherjee, S., Mehta, D., Dhangar, K., Kumar, M., 2021. Environmental fate, distribution and state-of-the-art removal of antineoplastic drugs: a comprehensive insight. Chem. Eng. J. 407, 127184.

National Centre for Biotechnology Information, 2022. PubChem compound summary. https://www.ncbi.nlm.nih.gov/, 2 Apirl 2024.

Ng, B., Quinete, N., Maldonado, S., Lugo, K., Purrinos, J., Briceño, H., Gardinali, P., 2021. Understanding the occurrence and distribution of emerging pollutants and endocrine disruptors in sensitive coastal South Florida Ecosystems. Sci. Total Environ. 757, 143720.

Ngeno, E., Ongulu, R., Orata, F., Matovu, H., Shikuku, V., Onchiri, R., Gichumbi, J., 2023. Endocrine disrupting chemicals in wastewater treatment plants in Kenya, East Africa: concentrations, removal efficiency, mass loading rates and ecological impacts. Environ. Res., 117076

Ngeno, E.C., Mbuci, K.E., Necibi, M.C., Shikuku, V.O., Olisah, C., Ongulu, R., Sillanpää, M., 2022. Sustainable re-utilization of waste materials as adsorbents for water and wastewater treatment in Africa: recent studies, research gaps, and way forward for emerging economies. Environmental Advances 9, 100282.

Ngeno, E.C., Orata, F.O., Baraza, L.D., Shikuku, V.O., Kimosop, S.J., 2016. Adsorption of Caffeine and Ciprofloxacin onto Pyrolitically derived water Hyacinth biochar: isothermal, kinetic and thermodynamic studies. Journal of Chemistry and Chemical Engineering 10, 185–194.

Ojoghoro, J., Scrimshaw, M., Sumpter, J., 2021. Steroid hormones in the aquatic environment. Sci. Total Environ. 792, 148306.

Ong, S.-T., Khoo, E.-C., Keng, P.-S., Hii, S.-L., Lee, S.-L., Hung, Y.-T., Ha, S.-T., 2011. Plackett–Burman design and response surface methodological approach to optimize basic dyes removal using sugarcane bagasse. Desalination Water Treat. 25, 310–318.

Ongulu, R.A., Kituyi, J.L., Getenga, Z.M., 2015. Biosorption of Pb^{2+} and Cr^{2+} using *Moringa oleifera* and their adsorption isotherms. Sci. J. Anal. Chem. 3, 100–108.

Orata, F., 2018. Conventional wastewater treatment plants as a discharge and source point for biota exposure to micro-pollutants. In: Ecotoxicology: Perspectives on Key Issues. CRC Press, p. 213.

Owino, E.K., Shikuku, V.O., Nyairo, W.N., Kowenje, C.O., Otieno, B., 2023. Valorization of solid waste incinerator fly ash by geopolymer production for removal of anionic bromocresol green dye from water: kinetics, Isotherms and Thermodynamics studies. Sustainable Chemistry for the Environment 3, 100026.

Ragab, D., Gomaa, H., Sabouni, R., Salem, M., Ren, M., Zhu, J., 2016. Micropollutants removal from water using microfiltration membrane modified with ZIF-8 metal organic frameworks (MOFs). Chem. Eng. J. 300, 273–279.

Redlich, O., Peterson, D.L., 1959. A useful adsorption isotherm. Journal of physical chemistry 63, 1024, 1024.

Salame, I.I., Bandosz, T.J., 2003. Role of surface chemistry in adsorption of phenol on activated carbons. J. Colloid Interface Sci. 264, 307–312.

Šauer, P., Stará, A., Golovko, O., Valentová, O., Bořík, A., Grabic, R., Kroupová, H.K., 2018. Two synthetic progestins and natural progesterone are responsible for most of

the progestagenic activities in municipal wastewater treatment plant effluents in the Czech and Slovak republics. Water Res. 137, 64–71.
Shikuku, V.O., Donato, F.F., Kowenje, C.O., Zanella, R., Prestes, O.D., 2015. A comparison of adsorption equilibrium, kinetics and thermodynamics of aqueous phase clomazone between faujasite X and a natural zeolite from Kenya. S. Afr. J. Chem. 68, 245–252.
Shikuku, V.O., Jemutai-Kimosop, S., 2020. Efficient removal of sulfamethoxazole onto sugarcane bagasse-derived biochar: two and three-parameter isotherms, kinetics and thermodynamics. S. Afr. J. Chem. 73, 111–119.
Shikuku, V.O., Zanella, R., Kowenje, C.O., Donato, F.F., Bandeira, N.M., Prestes, O.D., 2018. Single and binary adsorption of sulfonamide antibiotics onto iron-modified clay: linear and nonlinear isotherms, kinetics, thermodynamics, and mechanistic studies. Appl. Water Sci. 8, 1–12.
Sips, R.J., 1948. On the structure of a catalyst surface. J. Chem. Phys. 16, 490–495.
Treybal, R., 1981. Mass-transfer operations, McGraw-Hill. Using tree fern as a biosorbent. Process Biochem 40, 119–124.